Flexible and Stretchable Electronics for Biointegrated Devices

Dae-Hyeong Kim,[1] Roozbeh Ghaffari,[2] Nanshu Lu,[3] and John A. Rogers[4]

[1]School of Chemical and Biological Engineering, Institute of Chemical Processes, Seoul National University, Seoul 151-744, Korea

[2]MC10 Inc., Cambridge, Massachusetts 02140

[3]Department of Aerospace Engineering and Engineering Mechanics, University of Texas at Austin, Austin, Texas 78712

[4]Department of Materials Science and Engineering, Beckman Institute for Advanced Science and Technology, and Frederick Seitz Materials Research Laboratory, University of Illinois at Urbana-Champaign, Urbana, Illinois 61801; email: jrogers@uiuc.edu

Annu. Rev. Biomed. Eng. 2012. 14:113–28

First published online as a Review in Advance on April 18, 2012

The *Annual Review of Biomedical Engineering* is online at bioeng.annualreviews.org

This article's doi: 10.1146/annurev-bioeng-071811-150018

1523-9829/12/0815-0113$20.00

Keywords

electrophysiology, flexible electronics, semiconductor nanomaterials, human-machine interfaces, epilepsy, arrhythmia

Abstract

Advances in materials, mechanics, and manufacturing now allow construction of high-quality electronics and optoelectronics in forms that can readily integrate with the soft, curvilinear, and time-dynamic surfaces of the human body. The resulting capabilities create new opportunities for studying disease states, improving surgical procedures, monitoring health/wellness, establishing human-machine interfaces, and performing other functions. This review summarizes these technologies and illustrates their use in forms integrated with the brain, the heart, and the skin.

Contents

1. INTRODUCTION

All established classes of high-performance electronics exploit single-crystal inorganic materials, such as silicon or gallium arsenide, in forms (i.e., semiconductor wafers) that are fundamentally rigid and planar (1–6). The human body is, by contrast, soft and curvilinear. This mismatch in properties hinders the development of devices capable of intimate, conformal integration with biological tissues, for applications ranging from basic measurement of electrophysiological signals (7), to delivery of advanced therapies (8), to establishment of human-machine interfaces (9). One envisioned solution involves the use of organic electronic materials, whose flexible properties have generated interest in them for potential use in paper-like displays (10–12), solar cells (13–15), and other types of consumer electronic devices (16–18). Such materials are not, however, stretchable or capable of wrapping curvilinear surfaces; they also offer only moderate performance, with uncertain reliability and capacity for integration into complex integrated circuits. Other materials, such as inorganic semiconductor nanowires (19) and carbon nanotubes (20), offer some promise, but they remain in early stages of development.

Emerging design strategies and fabrication techniques that exploit conventional inorganic semiconductor materials in unconventional ways provide compelling alternatives (21, 22), with several recent examples of use in clinically relevant thin, stretchable tissue-like devices that noninvasively integrate with various organs of the body (23, 24). This class of technology, which we describe as biointegrated to reflect its mode of deployment, exploits high-quality monocrystalline semiconductor nanomaterials (e.g., membranes, ribbons) in mechanically optimized layouts on soft, elastomeric, or flexible substrates (25, 26). Transfer printing techniques (27) provide the basis for manufacturing such systems, in forms that allow facile, noninvasive lamination on biological surfaces, including those of the brain (24, 28), heart (23, 26), and skin (25). Key mechanics principles, such as neutral mechanical plane configurations (29, 30) and serpentine geometrical designs (22, 31), minimize strains in the active materials, whereas waterproof encapsulating films (26, 32) ensure long-term reliability. In advanced versions, bioresorbable substrates (e.g., silk) provide routes for intimate physical coupling to soft tissues, with negligible mechanical disturbance (24).

This review highlights the use of these ideas in diagnostic devices for brain surgery, interfaces for human-computer control systems (24, 28), skin-based physiological status monitors (25), and instrumented balloon catheter tools for cardiac ablation therapy (23). These examples demonstrate the ability of biointegrated devices to (*a*) map electrical, temperature, mechanical strain and flow profiles, (*b*) wirelessly supply power, (*c*) provide quantitative feedback via tactile sensing, (*d*) electrically or photodynamically stimulate tissues, and (*e*) ablate with fine spatial resolution. In all cases, the components for the systems have the high performance and reliability standards of established integrated circuit technologies. This review begins with a brief overview of the materials, mechanics, and manufacturing strategies. Discussions of applications separate into devices that mount on internal organs and on the skin. A concluding section provides some perspectives on future opportunities.

2. MATERIALS, PROCESSING TECHNIQUES, AND MECHANICS DESIGN

2.1. Semiconductor Nanomaterials

The processes for creating semiconductor nanomembranes/ribbons (which we refer to generally as NMs) begin with high-quality single-crystal wafers (**Figure 1*a***) of (111) silicon (top) (33–35), (100) silicon-on-insulator (SOI) (middle) (36–38), or epitaxially grown III–V semiconductors (bottom) (39, 40). Lithographic patterning procedures and chemical etching techniques define the lateral dimensions, configurations, and thicknesses (typically tens to hundreds of nanometers) of NMs that are released from such "source" wafers. The first route (**Figure 1*a***, top) uses anisotropic wet etching of (111) silicon with potassium hydroxide or tetramethyl ammonium hydroxide, both of which remove material along the surfaces of the wafers at much higher rates than into their depths (33–35). Coatings of silicon nitride or metal protect the sidewalls of the NMs from this etching. The second method (**Figure 1*a***, middle) exploits isotropic elimination of the buried silicon dioxide of SOI with hydrofluoric acid (HF) to free the top layer of silicon from the supporting wafer (36–38). The third approach (**Figure 1*a***, bottom) utilizes isotropic etching of sacrificial layers epitaxially formed in multilayer stacks (39, 40). As an example, thin films of GaAs, grown on sacrificial layers of AlAs, can be removed by selectively etching away the AlAs with HF. In the first and third techniques, the processes can be repeated to yield large quantities of high-quality NMs, in a repetitive manner or in a single, multilayer sequence (40). To prepare defect-free surfaces, chemical-mechanical planarization procedures and passivation methods, in adapted versions of steps already used in the semiconductor industry, can in many cases yield electrical properties in the NMs that are similar to those of unreleased films.

For present purposes, the NMs are useful because their small thicknesses yield extremely low bending stiffnesses (up to 15 orders of magnitude smaller than those of wafers) (41, 42) and low interfacial stresses in bonded configurations (up to 5 orders of magnitude) (31, 43). These characteristics allow NMs to be assembled, stacked, and heterogeneously integrated in ways that would be impossible with bulk materials (44). As a result, straightforward use of NMs enables flexible, and even stretchable, device designs. Manufacturing with NMs can be challenging, however, due to their small sizes and associated mechanical fragility. Recently developed techniques of transfer printing are thus critically important, as described next.

2.2. Transfer Printing

Transfer printing begins with a soft stamp made of an elastomer such as (poly)dimethylsiloxane (PDMS), designed to allow retrieval of NMs, released from their source wafer but tethered at

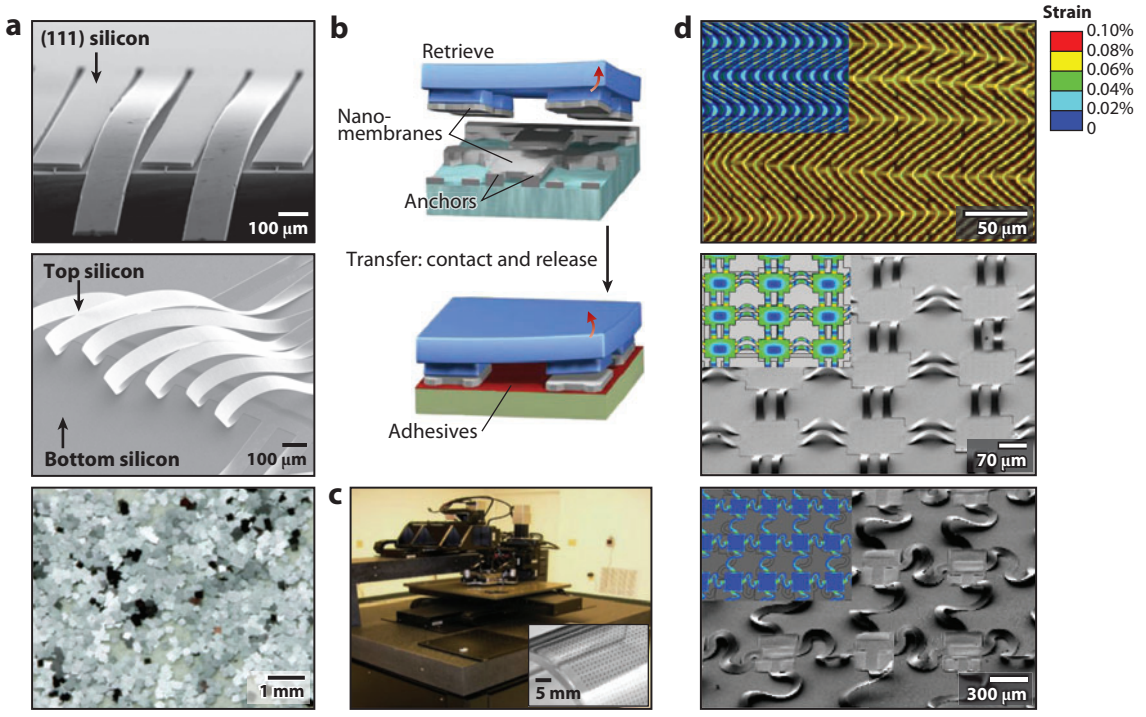

Figure 1

Materials, processing approaches, and layouts that yield stretchable forms of inorganic semiconductors such as silicon and gallium arsenide. (*a*) Nanomembranes of these materials, produced from high-quality, single-crystal wafers using lithographic patterning and etching. (*Top*) A set of flexible nanomembranes/ribbons (NMs) made of (111) silicon created by anisotropic undercut etching of a silicon wafer. (*Middle*) (100) silicon NMs released from a silicon-on-insulator wafer by removal of the buried oxide. (*Bottom*) A large collection of GaAs NMs prepared from epitaxial, multilayer stacks of GaAs/AlAs. Selectively etching the sacrificial AlAs layers releases GaAs NMs. Reproduced with permission from Reference 40. Copyright Nature Publishing Group. (*b*) Schematic of the process for transfer printing collections of NMs from their released forms on a source wafer to a target surface. Reproduced with permission from Reference 39. Copyright American Association for the Advancement of Science. (*c*) Automatic transfer printing tool. Inset shows a collection of GaAs NMs printed onto a flexible sheet of polyethylene terephthalate. (*d*) Scanning electron microscope images and (*insets*) corresponding finite element modeling results for semiconductor NMs bonded to prestrained elastomeric substrates in three different configurations. Upon releasing the prestrain, controlled buckling processes in the NMs lead to different layouts: (*top*) two-dimensional herringbone "wavy" patterns (reproduced with permission from Reference 37, copyright American Chemical Society) and noncoplanar bridge structures with (*middle*) straight and (*bottom*) serpentine (reproduced with permission from Reference 22, copyright National Academy of Sciences) interconnects. In all cases, strains in the silicon structures themselves are less than ~0.1%, even when strains of the overall system exceed 100% in certain configurations.

strategic points (i.e., anchors), simply by the action of generalized adhesion forces to the PDMS, typically dominated by van der Waals interactions (27, 45) (**Figure 1*b***, top). This transfer can be performed over large areas of uniform or segmented NMs using flat stamps (27) or over selected areas using structured stamps (46) (**Figure 1*b***, top). The retrieved collections of NMs (i.e., solid "inks" in this procedure) are selectively delivered to target substrate surfaces, at predefined locations with microscale precision (**Figure 1*b***, bottom), by printing (39, 47). A variety of approaches allow the switching in adhesion needed for efficient operation; these range from rate-dependent viscoelastic effects (27, 48), to biomimetic strategies (45), to use of interfacial bonding layers (49). Printing with automated tools that include high-resolution

cameras for overlay registration and multidimensional stages for positional control enables submicron-scale capabilities that are fully compatible with NMs and that offer throughputs of millions of individual NMs per hour (39, 40) (**Figure 1*c***). When used in a step-and-repeat manner, the process can disperse NMs over large areas in sparse and materials-efficient layouts matched to system requirements, many of which demand areal coverage that is much larger than that which can be cost-effectively addressed using conventional integrated circuit technology. **Figure 1*c*** (inset) shows a sparse array of printed GaAs NMs on a bent sheet of plastic (39).

When bonded to thin substrates, inorganic NMs provide routes to high-quality electronics and sensors capable of bending to small (<1 mm) radii of curvature (21, 28, 50). Nevertheless, even in these designs, the extreme bending (i.e., folding) and stretching/compressing that occur in many interfaces with the human body can lead to strains that exceed fracture thresholds in common inorganic materials (~1%) (41, 42). For example, electronics integrated on the human skin must undergo strains of up to 30% or more (51) without constraining natural motions. Sensors and electrodes on compliant or inflatable balloon catheters for minimally invasive surgical procedures require even higher levels of deformation, i.e., strains of well over 100% (23). A powerful strategy to accommodate such strains exploits the controlled physics of nonlinear buckling processes (36, 52). As a simple example of this idea, transfer printing an NM on a prestretched elastomeric substrate and then releasing this strain leads to compressive stresses that produce a herringbone pattern of buckling (37) (**Figure 1*d***, top). When the substrate is subsequently stretched by amounts less than the prestrain, the amplitudes and wavelengths of the buckled structures change in ways that maintain small, materials-level strains in the NM, thereby avoiding fracture. The same concepts can be applied with ultrathin, flexible integrated circuits. Advanced versions of this basic idea involve structuring the circuits into open mesh layouts and selectively bonding only the device island regions to the prestretched elastomer. In this case, the interconnects delaminate to adopt arc-shaped geometries upon release of the prestrain (22, 29, 31) (**Figure 1*d***, middle). When the system is subjected to deformation, the interconnects move freely in ways that both strain-isolate the devices and reduce the strains in the interconnect materials by orders of magnitude compared with those in the elastomer substrate (43). Further improvements are possible by using serpentine-shaped interconnects (**Figure 1*d***, bottom) in otherwise similar overall constructs.

3. FLEXIBLE AND STRETCHABLE ELECTRONICS AND OPTOELECTRONICS

3.1. Flexible Devices

One of the most powerful electronic components that can be constructed using the materials and processes described above is the field-effect transistor. **Figure 2*a*** (top inset) shows n-type (right) and p-type (left) silicon metal oxide semiconductor field-effect transistors (MOSFETs) (38). Doped NMs of silicon used with gate dielectric layers (SiO_2) and metal electrodes can achieve electrical performance on plastic substrates that is comparable to that of otherwise similar devices on rigid silicon wafers (38, 53, 54). Connection of n-type and p-type MOSFETs allows integrated circuits, for which complementary-MOS (CMOS) inverters (**Figure 2*a***, right-hand side) are key building blocks (38). Arranging CMOS inverters in series or in parallel configurations can yield various functions, such as that of the ring oscillator shown in **Figure 2*a*** (center). In this example, an ~25-μm-thick flexible sheet of polyimide serves as the substrate. Transfer printing various kinds of semiconductor materials in multiple layers enables even more sophisticated devices, in which active circuit elements in different layers can be interconnected through vias and edge-over metallization, yielding three-dimensional heterogeneous circuits (44) (**Figure 2*b***).

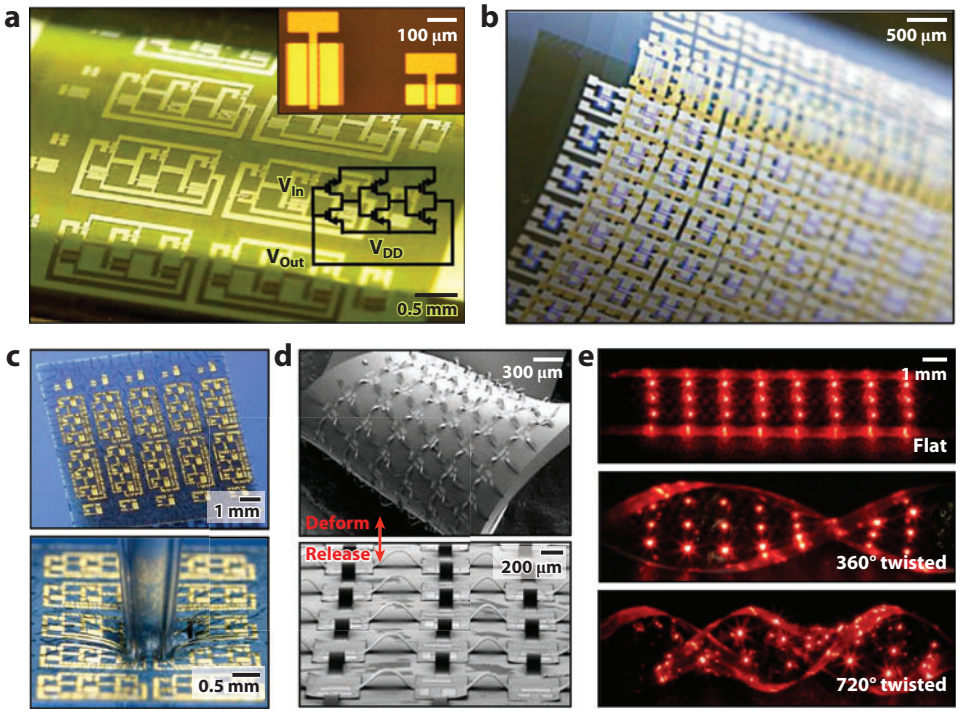

Figure 2

Flexible and stretchable electronic and optoelectronic devices. (*a*) Flexible circuit with transistors that use silicon nanomembranes/ribbons (NMs) on a 25-μm-thick polyimide substrate: (*left* and *top inset*) n-type and and p-type transistors, (*right*) complementary metal oxide semiconductor (CMOS) inverters, and (*center*) three-stage ring oscillators. (*a*, *bottom inset*) A circuit diagram of a ring oscillator. Abbreviations: V_{In}, input voltage; V_{Out}, output voltage; V_{DD}, power supply voltage. Reproduced with permission from Reference 38. Copyright IEEE. (*b*) Three-dimensional, multilayer circuit on a plastic substrate formed by repeated cycles of transfer printing and device processing. (*c*) Stretchable CMOS circuit that uses a "wavy" layout on an elastomeric substrate shown (*top*) before and (*bottom*) during application of normal force with a glass rod. Reproduced with permission from Reference 21. Copyright American Association for the Advancement of Science. (*d*) Scanning electron microscope images of a (*top*) deformed and (*bottom*) undeformed collection of CMOS inverters that use straight, noncoplanar interconnects. A thin (~1 mm) elastomer membrane serves as the substrate. Reproduced with permission from Reference 22. Copyright National Academy of Sciences. (*e*) Stretchable array of GaAs microscale inorganic light-emitting diodes with serpentine interconnects in flat, 360° twisted, and 720° twisted states. Reproduced with permission from Reference 32. Copyright Nature Publishing Group.

3.2. Stretchable Devices

Electronic systems can also be achieved on stretchable substrates. **Figure 2*c*** shows CMOS circuits on PDMS, capable of reversible elastic responses to significant mechanical deformations, by virtue of the buckling mechanics described previously (21). This type of system forms when an ultrathin (less than ~3 μm) CMOS silicon circuit, transferred onto a biaxially prestretched PDMS, buckles as a result of releasing the prestrain (**Figure 1*d***) to adopt generalized versions of the herringbone layouts shown in **Figure 1*d*** (top). The circuits in this case lie between two identical polyimide layers in the neutral mechanical plane to minimize bending-induced strains. When mildly stretched, the

devices and interconnects gradually flatten in a way that avoids significant strains in the active materials or associated changes in performance.

As an example of a device of more advanced design, **Figure 2*d*** shows an array of CMOS inverters with noncoplanar, arc-shaped interconnects under deformation (22). Similar interconnects, but with serpentine shapes, further increase the stretchability. **Figure 2*e*** shows twisting deformations (by up to 720°) in an interconnected array of microscale inorganic light-emitting diodes (μ-ILEDs) built using these ideas (32). This type of mechanical response suggests an ability to wrap complex curvilinear and time-dynamic surfaces, such as those found in biology. The remaining sections highlight some examples; each begins with an overview of the existing state of the art.

4. BIOINTEGRATED DEVICES ON INTERNAL ORGANS

4.1. Integrating with the Brain

High-resolution neural interface devices have played important roles in brain and central nervous system research over the past decades (55). Electrical recordings performed with penetrating (56) or surface-contacting electrodes (57) have dramatically improved our understanding of the basic science of neural activity; they have also been exploited for clinical usage in epilepsy surgery (58–60), prosthetic control (9), and other applications (61). Extensive reviews of electrode arrays used in surgical procedures to treat epilepsy appear elsewhere (62, 63). Briefly, such devices often consist of a relatively small number of large electrodes (e.g., ∼6-mm diameters and ∼1-cm spacings) on flexible sheets that contact the surface of the brain to collect neural signals generated by clusters of neurons (57). Although the large area coverage provided by such technologies is attractive in terms of gaining valuable information about precise brain activity and foci triggers of disease states, such as epilepsy, the spatial density of electrodes should be as high as possible, with spacings of ∼400 μm or less (64). Electrode arrays positioned underneath the dura membrane and in direct contact with cortical surfaces can combine macroelectrodes with microwires (58–60) to achieve this improved resolution. The number of wire connections required in these types of passive systems, however, imposes practical constraints that preclude the possibility of simultaneous large-area and high-resolution operation (28).

Multiplexing circuits provide a solution that reduces the number of required connections for n electrodes, from n to sqrt(n). For example, a 16×16 array of electrodes requires ∼30 wires with multiplexers, compared with ∼260 wires in passive configurations. The significance of this reduction increases rapidly with electrode count. The challenge with multiplexing is that the required electronics, in conventional forms, are rigid and flat, thereby rendering them incompatible with the soft, curved textures of the brain (65). One widely used approach bypasses this constraint by use of penetrating electrode pins that terminate on flat platforms, suitable for mounting of conventional silicon integrated circuits (64, 66, 67). The Utah array represents a prominent and successful example of this strategy (64, 66), where the pins provide access to clusters of neurons in a way that also overcomes the mismatches in geometry. An important disadvantage is that tissue damage caused by electrode insertion and continued irritation during long-term implantation (due to micromovement of brain tissue) can trigger adverse effects, including astrocyte proliferation and inflammation, both of which lead to signal degradation over time (68).

An alternative involves collections of diced silicon chips, each of which supports planar electrodes with hemispherical bumps and multiplexing electronics, bonded to plastic sheets (69). This approach can be effective, but there are significant challenges due to the inflexibility and relatively large sizes of the chips. Reduction of stiffness is crucial for achieving systems that not only are safe but also provide high-fidelity data streams (24). Flexible electronics using the NM concepts

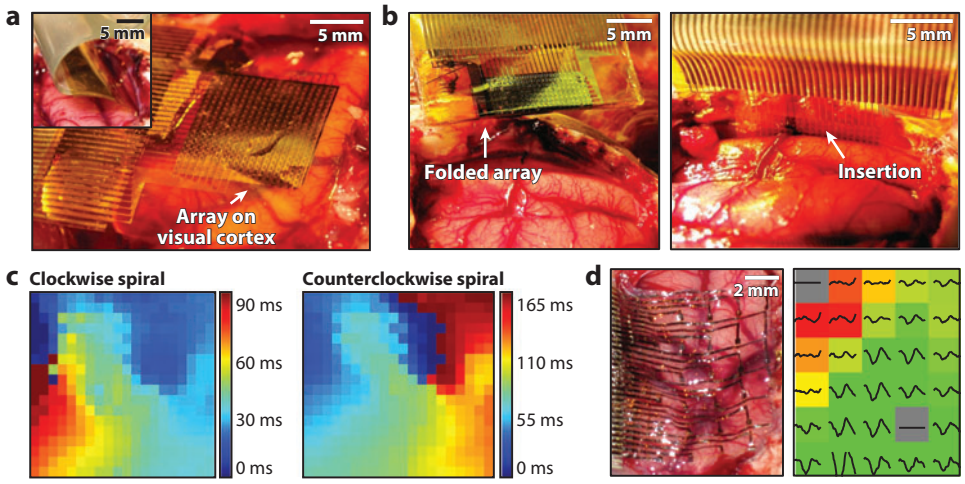

Figure 3

High-density, conformal electrode array for brain surface recording. (*a*) High-density device with multiplexers based on silicon nanomembranes/ribbons. Inset shows a similar array folded around a thin (~700 μm) elastomer sheet and inserted into an interhemispheric fissure. (*b*) Images (*left*) before and (*right*) after insertion. (*c*) Local administration of picrotoxin into the visual cortex causes spiral wave fronts that can be seen clearly in recordings from the high-density array. Reproduced with permission from Reference 28. Copyright Nature Publishing Group. (*d*) (*left*) Image and (*right*) mapping results of an ultrathin (~2.5 μm) mesh electrode array laminated onto the surface of the brain following dissolution of a temporary silk substrate. The mesh design enables exceptionally good conformal contact, and thus higher quality in the measured signals compared with that possible with conventional flexible arrays. Reproduced with permission from Reference 24. Copyright Nature Publishing Group.

described previously permit high-speed multiplexing, high temporal resolution, as well as conformal electrode-tissue interfaces over large areas (28) (**Figure 3*a***). The thin form factor and low stiffness even offer direct mechanical access to the hemispherical fissure area of the brain (**Figure 3*a***, inset). Folded electrode arrays enable simultaneous mapping from both sides of the hemispheres (**Figure 3*b***). Furthermore, high-density systems with submillimeter spacing between the electrodes yield insights into new neural mechanisms, whereby unusual clockwise and counterclockwise spiral patterns of excitation propagate in a manner correlated to signs of microseizures (28, 70) (**Figure 3*c***).

Even fully flexible electrode arrays such as these may not, however, make complete conformal contact with the most topologically demanding regions of the human brain (24) (**Figure 3*d***). Reducing thicknesses to less than ~10 μm, and structuring the sheets into open mesh geometries, can improve the coupling (**Figure 3*d***). To enable mechanical manipulation for mounting such systems, which themselves are difficult to handle due to their extremely low bending stiffnesses, sacrificial substrates of materials (e.g., silk) that readily dissolve in biofluids can be useful. Once deployed on soft tissue, the silk dissolves leaving behind an ultrathin mesh of electrodes in intimate mechanical contact with even the most strongly curved/textured regions of the brain surface (24).

4.2. Integrating with the Heart

As with the brain, mapping electrical activity across the surface of the heart is important not only for developing a fundamental understanding of disease states but also for diagnosing local

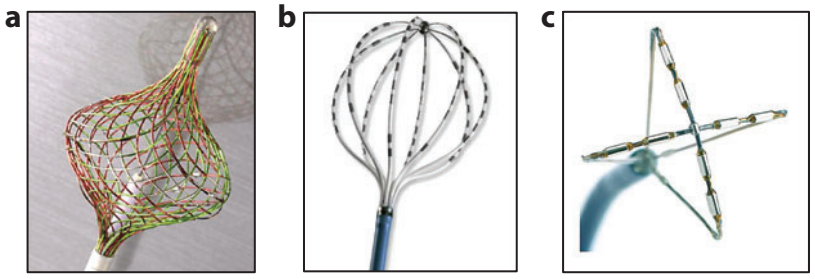

Figure 4

Multielectrode catheters for cardiac mapping and ablation. (*a*) Multielectrode mapping and ablation catheter (HD Mesh Ablator™, Bard; Lowell, MA) consists of 36 electrodes in mesh geometry, which optimizes contact with the pulmonary veins. (*b*) Multielectrode basket catheter (Constellation™, Boston Scientific; Boston, MA) provides high-density mapping of electrical activity within the atria. (*c*) Multielectrode mapping and ablation catheter (MAAC™, Medtronic; Minneapolis, MN) targets complex fractionated atrial electrograms for both mapping and ablation of the atrial body.

tissue behavior during certain surgical operations. Existing approaches use single-point electrical mapping catheters; newer systems exploit arrays of electrodes integrated on catheter-type delivery systems (8, 71). In both cases, clinical use in the context of treating certain types of arrhythmias often involves measurement of electrical potentials, in a point-by-point, manual fashion from locations within the ostium of the pulmonary veins (PVs) (where the PV is conjoined with the atria) (**Figure 4*a***) and within the atria (**Figure 4*b*,*c***). Positioning the catheters requires significant time and dexterity, often leading to inconsistent outcomes across multiple patients (71, 72). Furthermore, several sequential therapeutic procedures, such as ablation, followed by cycles of electrical mapping are required to produce a representation of electrical activity over a large region of interest (8, 71). This serial approach requires highly skilled operators to minimize risk of stroke and other clinical complications. In addition to atrial fibrillation treatment (73), catheters are used as tools for ablation in minimally invasive strategies for treating various forms of other cardiac arrhythmias, including ventricular fibrillation (74) and ventricular tachycardia (75). Linear lesions generated by radiofrequency energy applied in a point-by-point manner are among the most common means to correct these abnormal rhythms (71, 76).

Another way to enhance the performance of cardiac ablation solutions is to develop contact-sensing feedback and multielectrode catheter systems, which can improve electrical mapping of complex arrhythmias and provide real-time force feedback during lesion formation (77). Emerging balloon catheter–based systems also under development and in clinical trials rely on balloon substrates to conform to the anatomical structure of the PV ostium (8, 71, 78–83). These balloons inflate within the left atrium and create a continuous ring of conformal contact between the balloon and the tissue, followed by delivery of cryoenergy, high-intensity focused ultrasound (HIFU)–, or laser-based ablation therapies. Although conceptually straightforward, such balloon ablation catheters do not provide sensory feedback about mechanical contact with soft tissue or information on the electrical state of intracardiac surfaces.

Advances in stretchable electronics enable integration of contact sensors, multielectrode arrays, and balloon substrates into a single, multifunctional instrumented catheter platform (23). A representative example of a device of this type appears in **Figure 5**. Electrodes for electrical mapping integrate on the balloon surface with classes of serpentine interconnects described previously (**Figure 5*a*,*b***). **Figure 5*c*** shows temperature sensors and stretchable arrays of μ-ILEDs. Electrogram recordings from an inflated balloon substrate positioned in direct

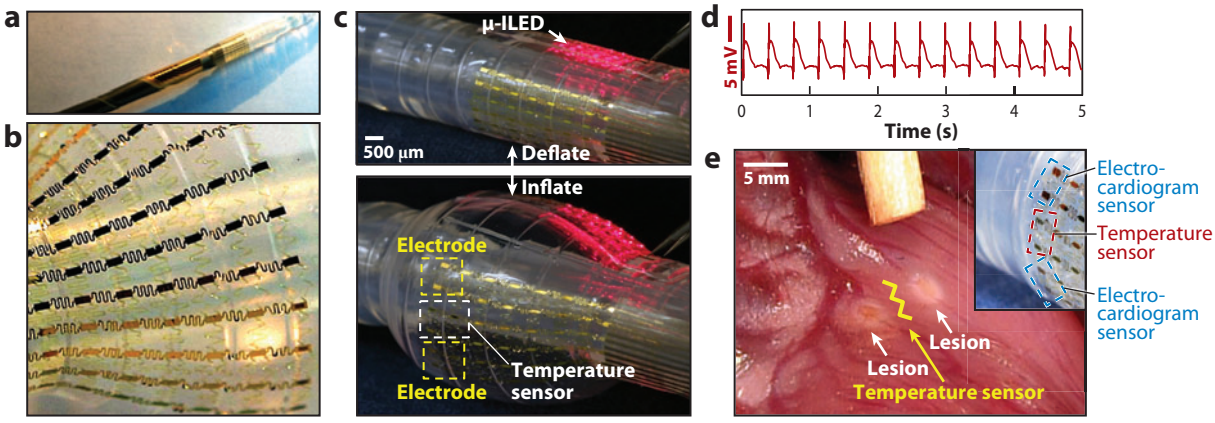

Figure 5

Multifunctional balloon catheter. (*a*) Stretchable sensors mounted on a catheter balloon and (*b*) magnified view showing stretched (~120%) serpentine interconnects after inflation. (*c*) Device in the deflated and inflated states, showing several different functionalities, ranging from electrodes for electrophysiological measurement and radiofrequency (RF) ablation to temperature sensors, contact force gauges, and arrays of microscale inorganic light-emitting diodes (μ-ILEDs). (*d*) Electrical recordings from the right ventricle of a rabbit heart, measured with an instrumented balloon catheter. (*e*) Lesions created by RF ablation electrodes on a similar device. Yellow line denotes the location of a temperature sensor. The inset provides a corresponding image of RF ablation electrodes and temperature sensors on the balloon catheter. Reproduced with permission from Reference 23. Copyright Nature Publishing Group.

mechanical contact with a live porcine heart are presented in **Figure 5*d***. This mode of operation is particularly useful for balloon ablation catheters, where assessment of ablation can be achieved quickly without the need for separate diagnostic devices. In addition to electrical and temperature sensors, contact sensors and stimulation electrodes (**Figure 5*e***) are also supported on this platform. Contact sensors can report the moment when the balloon skin and endocardial tissue touch, thereby providing important feedback (without X-ray imaging) on how to adjust and maneuver inflated balloons to achieve optimal occlusion of the PVs during ablation procedures.

More advanced biointegrated mapping systems have been demonstrated in epicardial sheets, designed in ultrathin formats described previously to allow conformal contact to and adhesion with the surface of the heart (26). Here, high-density electrodes, each with local amplifiers and multiplexing circuitry based on silicon NMs, enable measurements with both high spatial and temporal resolution. **Figure 6*a*** shows an image of a flexible mapping array with multiplexed electrodes, adherent on a section of cardiac tissue through surface tension forces alone without penetrating pins or separate adhesives. Electrograms collected at high sampling rates (12.5 kHz per electrode) and combined spatiotemporally across 288 electrodes yield isochronal activation maps, demonstrating the natural electrophysiology of the heart (**Figure 6*b***) in a noninvasive manner. These high-density arrays map activation patterns across entire regions of the heart, without manual operation or repositioning, in a single beat cycle. Furthermore, their thin form factor and mechanical reliability permit packaging in medical instruments, like the sorts of catheters described previously, for endocardial purposes.

5. BIOINTEGRATED DEVICES ON THE SKIN

Although biointegrated electronics on internal tissues provide important functions, the skin represents a mounting location that is applicable outside of hospital settings to allow much broader modes of use (84). Traditional technologies use small numbers of point-contact electrodes that

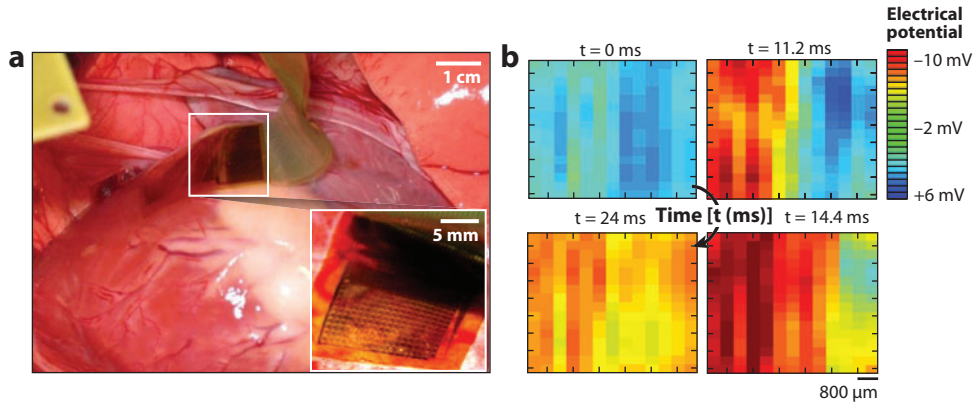

Figure 6

High-density, conformal electrode array for cardiac surface recording. (*a*) Sensor array with embedded multiplexing circuits and amplifiers based on silicon nanomembranes/ribbons conformally laminated on the epicardial surface of a live porcine heart. Inset shows a magnified view. (*b*) Activation patterns of depolarization mapped at four different time frames. The recorded electrical potential is converted into isochronal maps of activation patterns. Reproduced with permission from Reference 26. Copyright American Association for the Advancement of Science.

strap onto or penetrate through the surface of the skin (85, 86). For example, commercial devices for recording electroencephalograms (EEGs) from the scalp use tight caps embedded with electrodes, each of which attaches to external electronics via bulk wires (87). In this case and in others for measurement of ECG or electromyography (EMG), the skin is often prepared by light abrasion and application of conductive gel or paste as a means to reduce the contact impedance (88). Such procedures are time-consuming and also unsuitable for long-term recording. As a result, dry electrodes are of interest. Examples include micromachined pins (89) or arrays of carbon nanotubes (90) that allow penetration through the stratum corneum. This mode of integration has certain advantages over gels, but it can cause inflammation and discomfort (91). Capacitive coupling provides an attractive option that eliminates contact entirely (92). To minimize signal attenuation and channel gain mismatch, the input capacitance of each sensor must be actively neutralized using positive feedback and bootstrapping.

These systems have many important capabilities, but in general they are poorly suited for practical application outside of clinical research due to their bulky size and difficulties in establishing robust, nonirritating electrical contacts (93). Recently developed stretchable device technologies, referred to as epidermal electronic systems (EES), allow electrophysiological measurements with ultrathin and low-modulus, skin-like sheets that conformally laminate onto the surface of the skin in a manner that is mechanically invisible to the user, much like a temporary transfer tattoo (25) (**Figure 7*a***). The EES attaches intimately and physically couples to rough skin surfaces, via van der Waals forces alone, as shown in the cross-sectional confocal micrographs in **Figure 7*b***. Because attachment does not require separate adhesives or conductive gels, these systems can function for prolonged periods. EEG measurements using an EES mounted on the forehead are shown in **Figure 7*c***: The bottom frame presents a spectrogram showing an alpha rhythm; the top left frame shows a plot of discrete Fourier transform coefficients at ∼10 Hz. The patterns correspond to periods with the eyes closed and opened. The responses at ∼10 s and ∼14 s result from eye opening and blinking, respectively. The top right frame reveals Stroop effects (94), as an additional illustration of functionality of this technology. These and other electrophysiological

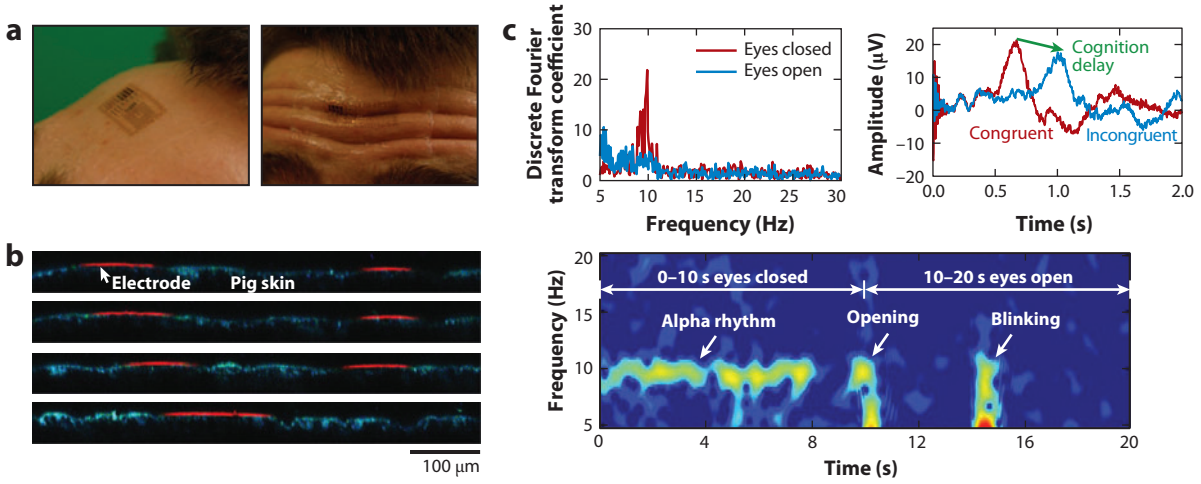

Figure 7

Epidermal electronic system (EES). (*a*) Images of an EES mounted on the forehead (*left*) without deformation and (*right*) under compression. (*b*) Cross-sectional confocal micrographs of the contacting interface between an EES and a piece of pig skin. (*c*) (*Top left*) Spectrogram of an electroencephalogram measured from the forehead and (*bottom*) corresponding frequency-versus-time plot. Expected alpha rhythms, with frequencies of ~10 Hz, appear for the first 10 s with the eyes closed. This response disappears after opening the eyes. (*Top right*) Evidence of the Stroop effect, which corresponds to a pattern of cognition delay during display of incongruent words and colors. Reproduced with permission from Reference 25. Copyright American Association for the Advancement of Science.

measurements (e.g., EMG, ECG) suggest utility not only in health/wellness monitoring but also in brain-machine interfaces, consumer and gaming applications, and other areas.

6. CONCLUSIONS

The advances summarized in this review offer immediate opportunities in many branches of biomedical science and engineering, with important end applications in clinical, research, and consumer domains. These directions emerge directly from the unique ability of these technologies to intimately and noninvasively integrate with the soft, curvilinear tissues of the body in ways that are impossible with conventional, wafer-based forms of electronics. Although the functions achieved thus far rely on diverse, physical modes of interaction with tissue, future systems might also incorporate biochemical coupling, for which new sensors and microelectromechanical and microfluidic components in flexible/stretchable formats will be required. Innovative ideas in materials and device engineering will be required, as will an improved fundamental understanding of the physical chemistry of the biotic/abiotic interface. Other areas for research include development of components for mechanical, thermal, or chemical energy scavenging and of systems for wireless communications. These engineering goals, the foundational science that underpins them, and their relevance to improvements in human health will drive interest in this emerging field for many years to come.

DISCLOSURE STATEMENT

J.A.R. and R.G. are cofounders of MC10, which pursues the commercialization of biointegrated devices.

ACKNOWLEDGMENTS

This material is based upon work supported by the Department of Defense, the National Science Foundation, and the Department of Energy. N.L. acknowledges support from a Beckman Institute postdoctoral fellowship. This work is also supported by Global Frontier Research Center for Advanced Soft Electronics.

LITERATURE CITED

1. Moore G. 1965. Cramming more components onto integrated circuits. *Electronics* 38:114–17
2. Arns RG. 1998. The other transistor: early history of the metal-oxide semiconductor field-effect transistor. *Eng. Sci. Educ. J.* 7:233–40
3. Vogel EM. 2007. Technology and metrology of new electronic materials and devices. *Nat. Nanotechnol.* 2:25–32
4. International Technology Roadmap for Semiconductors. 2011. **http://www.itrs.netLinks/2011ITRS/Home2011.htm**
5. Streetman BG, Banerjee S. 2005. *Solid State Electronic Devices*. Upper Saddle River, NJ: Prentice Hall. 6th ed.
6. Hayashi I. 1993. Optoelectronic devices and material technologies for photo-electronic integrated systems. *Jpn. J. Appl. Phys.* 32:266–71
7. Interwoven W. 1901. Un nouveau galvanometer. *Arch. Neerl. Sc. Ex. Nat.* 6:625–33
8. Dewire J, Calkins H. 2010. State-of-the-art and emerging technologies for atrial fibrillation ablation. *Nat. Rev. Cardiol.* 7:129–38
9. Hochberg LR, Serruya MD, Friehs GM, Mukand JA, Saleh M, et al. 2006. Neuronal ensemble control of prosthetic devices by a human with tetraplegia. *Nature* 442:164–71
10. Forrest SR. 2004. The path to ubiquitous and low-cost organic electronic appliances on plastic. *Nature* 428:911–18
11. Rogers JA, Bao Z, Baldwin K, Dodabalapur A, Crone B, et al. 2001. Paper-like electronic displays: large-area rubber-stamped plastic sheets of electronics and microencapsulated electrophoretic inks. *Proc. Natl. Acad. Sci. USA* 9:4835–40
12. Gelinck GH, Huitema HEA, Veenendaal EV, Cantatore E, Schrijnemakers L, et al. 2004. Flexible active-matrix displays and shift registers based on solution-processed organic transistors. *Nat. Mater.* 3:106–10
13. Yu G, Gao J, Hummelen JC, Wudi F, Heeger AJ. 1995. Polymer photovoltaic cells: enhanced efficiencies via a network of internal donor-acceptor heterojunctions. *Science* 270:1789–91
14. Kim JY, Lee K, Coates NE, Moses D, Nguyen TQ, et al. 2007. Efficient tandem polymer solar cells fabricated by all-solution processing. *Science* 317:222–25
15. Shaheen SE, Ginley DS, Jabbour GE. 2005. Organic-based photovoltaics: toward low-cost power generation. *MRS Bull.* 30:10–22
16. Ouyang J, Chu CW, Szmanda CR, Ma L, Yang Y. 2004. Programmable polymer thin film and non-volatile memory device. *Nat. Mater.* 3:918–22
17. Baude PF, Ender DA, Haase MA, Kelley TW, Muyres DV, et al. 2003. Pentacene-based radio-frequency identification circuitry. *Appl. Phys. Lett.* 82:3964–66
18. Cantatore E, Geuns TCT, Gelinck GH, Veenendaal E, Gruijthuijsen AFA, et al. 2007. A 13.56-MHz RFID system based on organic transponders. *IEEE J. Solid-State Circuits* 42:84–92
19. Tian B, Cohen-Karni T, Qing Q, Duan X, Xie P, et al. 2010. Three-dimensional, flexible nanoscale field-effect transistors as localized bioprobes. *Science* 329:831–34
20. Keefer EW, Botterman BR, Romero MI, Rossi AF, Gross GW. 2008. Carbon nanotube coating improves neuronal recordings. *Nat. Nanotechnol.* 3:434–39
21. Kim DH, Ahn JH, Choi WM, Kim HS, Kim TH, et al. 2008. Stretchable and foldable silicon integrated circuits. *Science* 320:507–11
22. Kim DH, Song J, Choi WM, Kim HS, Kim RH, et al. 2008. Materials and noncoplanar mesh designs for integrated circuits with linear elastic responses to extreme mechanical deformations. *Proc. Natl. Acad. Sci. USA* 105:18675–80

23. Kim DH, Lu N, Ghaffari R, Kim YS, Lee SP, et al. 2011. Materials for multifunctional balloon catheters with capabilities in cardiac electrophysiological mapping and ablation therapy. *Nat. Mater.* 10:316–23
24. Kim DH, Viventi J, Amsden JJ, Xiao J, Vigeland L, et al. 2010. Dissolvable films of silk fibroin for ultrathin, conformal biointegrated electronics. *Nat. Mater.* 9:511–17
25. Kim DH, Lu N, Ma R, Kim YS, Kim RH, et al. 2011. Epidermal electronics. *Science* 333:838–43
26. Viventi J, Kim DH, Moss JD, Kim YS, Blanco JA, et al. 2010. A conformal, bio-interfaced class of silicon electronics for mapping cardiac electrophysiology. *Sci. Transl. Med.* 2:24ra22
27. Meitl MA, Zhu ZT, Kumar V, Lee KJ, Feng X, et al. 2006. Transfer printing by kinetic control of adhesion to an elastomeric stamp. *Nat. Mater.* 5:33–38
28. Viventi J, Kim DH, Vigeland L, Frechette ES, Blanco JA, et al. 2011. Flexible, foldable, actively multiplexed, high-density electrode array for mapping brain activity in vivo. *Nat. Neurosci.* 14:1599–605
29. Ko HC, Stoykovich MP, Song J, Malyarchuk V, Choi WM, et al. 2008. A hemispherical electronic eye camera based on compressible silicon optoelectronics. *Nature* 454:748–53
30. Jung I, Xiao J, Malyarchuk V, Lu C, Li M, et al. 2011. Dynamically tunable hemispherical electronic eye camera system with adjustable zoom capability. *Proc. Natl. Acad. Sci. USA* 108:1788–93
31. Kim DH, Liu Z, Kim YS, Wu J, Song J, et al. 2009. Optimized structural designs for stretchable silicon integrated circuits. *Small* 5:2841–47
32. Kim RH, Kim DH, Xiao J, Kim BH, Park SI, et al. 2010. Waterproof AlInGaP optoelectronics on stretchable substrates with applications in biomedicine and robotics. *Nat. Mater.* 9:929–37
33. Mack S, Meitl MA, Baca AJ, Zhu ZT, Rogers JA. 2006. Mechanically flexible thin-film transistors that use ultrathin ribbons of silicon derived from bulk wafers. *Appl. Phys. Lett.* 88:213101
34. Baca AJ, Meitl MA, Ko HC, Mack S, Kim HS, et al. 2007. Printable single-crystal silicon micro/nanoscale ribbons, platelets and bars generated from bulk wafers. *Adv. Funct. Mater.* 17:3051–62
35. Ko HC, Baca AJ, Rogers JA. 2006. Bulk quantities of single-crystal silicon micro/nanoribbons generated from bulk wafers. *Nano Lett.* 6:2318–24
36. Khang DY, Jiang H, Huang Y, Rogers JA. 2006. A stretchable form of single crystal silicon for high performance electronics on rubber substrates. *Science* 311:208–12
37. Choi WM, Song J, Khang DY, Jiang H, Huang YY, et al. 2007. Biaxially stretchable "wavy" silicon nanomembranes. *Nano Lett.* 7:1655–63
38. Kim DH, Ahn JH, Kim HS, Lee KJ, Kim TH, et al. 2008. Complementary logic gates and ring oscillators on plastic substrates by use of printed ribbons of single-crystalline silicon. *IEEE Electron Device Lett.* 29:73–76
39. Park SI, Xiong Y, Kim RH, Elvikis P, Meitl M, et al. 2009. Printed assemblies of inorganic light-emitting diodes for deformable and semitransparent displays. *Science* 325:977–81
40. Yoon J, Jo S, Chun IS, Jung I, Kim HS, et al. 2010. GaAs photovoltaics and optoelectronics using releasable multilayer epitaxial assemblies. *Nature* 465:329–33
41. Rogers JA, Someya T, Huang Y. 2010. Materials and mechanics for stretchable electronics. *Science* 327:1603–7
42. Rogers JA, Lagally MG, Nuzzo RG. 2011. Synthesis, assembly and applications of semiconductor nanomembranes. *Nature* 477:45–53
43. Kim DH, Kim YS, Wu J, Liu Z, Song J, et al. 2009. Ultrathin silicon circuits with strain-isolation layers and mesh layouts for high-performance electronics on fabric, vinyl, leather, and paper. *Adv. Mater.* 21:3703–7
44. Ahn JH, Kim HS, Lee KJ, Jeon S, Kang SJ, et al. 2006. Heterogeneous three dimensional electronics using printed semiconductor nanomaterials. *Science* 314:1754–57
45. Kim S, Wu J, Carlson A, Jin SH, Kovalsky A, et al. 2010. Microstructured elastomeric surfaces with reversible adhesion and examples of their use in deterministic assembly by transfer printing. *Proc. Natl. Acad. Sci. USA* 107:17095–100
46. Kim TH, Choi WM, Kim DH, Meitl MA, Menard E, et al. 2008. Printable, flexible, and stretchable forms of ultrananocrystalline diamond with applications in thermal management. *Adv. Mater.* 20:2171–76
47. Kim H, Brueckner E, Song J, Li Y, Kim S, et al. 2011. Unusual strategies for using indium gallium nitride grown on silicon (111) for solid-state lighting. *Proc. Natl. Acad. Sci. USA* 108:10072–77

48. Feng X, Meitl MA, Bowen AM, Huang Y, Nuzzo RG, et al. 2007. Competing fracture in kinetically controlled transfer printing. *Langmuir* 23:12555–60
49. Sun Y, Rogers JA. 2007. Structural forms of single crystal semiconductor nanoribbons for high-performance stretchable electronics. *J. Mater. Chem.* 17:832–40
50. Park SI, Le AP, Wu J, Huang Y, Li X, et al. 2010. Light emission characteristics and mechanics of foldable inorganic light-emitting diodes. *Adv. Mater.* 22:3062–66
51. Pailler-Mattei C, Bec S, Zahouani H. 2008. In vivo measurements of the elastic mechanical properties of human skin by indentation tests. *Med. Eng. Phys.* 30:599–606
52. Sun Y, Choi WM, Jiang H, Huang Y, Rogers JA. 2006. Controlled buckling of semiconductor nanoribbons for stretchable electronics. *Nat. Nanotechnol.* 1: 201–7
53. Ahn JH, Kim HS, Lee KJ, Zhu ZT, Menard E, et al. 2006. High speed, mechanically flexible single-crystal silicon thin-film transistors on plastic substrates. *IEEE Electron Device Lett.* 27:460–62
54. Ahn JH, Kim HS, Menard E, Lee KJ, Zhu ZT, et al. 2007. Bendable integrated circuits on plastic substrates by use of printed ribbons of single-crystalline silicon. *Appl. Phys. Lett.* 90:213501
55. Ryu SI, Shenoy KV. 2009. Human cortical prostheses: Lost in translation? *Neurosurg. Focus* 27:E5
56. Nicolelis MAL, Dimitrov D, Carmena JM, Crist R, Lehew G, et al. 2003. Chronic, multisite, multielectrode recordings in macaque monkeys. *Proc. Natl. Acad. Sci. USA* 100:11041–46
57. Schalk G, Miller KJ, Anderson NR, Wilson JA, Smyth MD, et al. 2008. Two-dimensional movement control using electrocorticographic signals in humans. *J. Neural Eng.* 5:75–84
58. Worrell GA, Gardner AB, Stead SM, Hu S, Goerss S, et al. 2008. High-frequency oscillations in human temporal lobe: simultaneous microwire and clinical macroelectrode recordings. *Brain* 131:928–37
59. Asano E, Juhasz C, Shah A, Sood S, Chugani HT. 2009. Role of subdural electrocorticography in prediction of long-term seizure outcome in epilepsy surgery. *Brain* 132:1038–47
60. Stead M, Bower M, Brinkmann BH, Lee K, Marsh WR, et al. 2010. Microseizures and the spatiotemporal scales of human partial epilepsy. *Brain* 133:2789–97
61. Perlmutter JS, Mink JW. 2006. Deep brain stimulation. *Annu. Rev. Neurosci.* 29:229–57
62. Stacey WC, Litt B. 2008. Technology insight: neuroengineering and epilepsy—designing devices for seizure control. *Nat. Clin. Pract. Neurol.* 4:190–201
63. Halpern CH, Samadani U, Litt B, Jaggi JL, Baltuch GH. 2008. Deep brain stimulation for epilepsy. *Neurotherapeutics* 5:59–67
64. Campbell PK, Jones KE, Huber RJ, Horch KW, Normann RA. 1991. A silicon-based, 3-dimensional neural interface—manufacturing process for an intracortical electrode array. *IEEE Trans. Biomed. Eng.* 38:758–68
65. Patterson WR, Song YK, Bull CW, Ozden I, Deangellis AP, et al. 2004. Modeling of elastic evolution of cirrhotic human liver. *IEEE Trans. Biomed. Eng.* 51:1854–56
66. Kim S, Bhandari R, Klein M, Negi S, Rieth L, et al. 2009. Integrated wireless neural interface based on the Utah electrode array. *Biomed. Microdevices* 11:453–66
67. Drake KL, Wise KD, Farraye J, Anderson DJ, BeMent SL. 1988. Performance of planar multisite microbes in recording extracellular single-unit intracortical activity. *IEEE Trans. Biomed. Eng.* 35:719–33
68. Griffith RW, Humphrey DR. 2006. Neuroprotective effect of FK506, an immunosuppressant, on transient global ischemia in gerbil. *Neurosci. Lett.* 206:81–84
69. Tokuda T, Pan YL, Uehara A, Kagawa K, Nunoshita M, et al. 2005. Flexible and extendible neural interface device based on cooperative multi-chip CMOS LSI architecture. *Sens. Actuators A* 122:88–98
70. Huang X, Xu W, Liang J, Takagaki K, Gao X, et al. 2010. Spiral wave dynamics in neocortex. *Neuron* 9:978–90
71. Calkins H, Brugada J, Packer DL, Cappato R, Chen SA, et al. 2007. HRS/EHRA/ECAS expert consensus statement on catheter and surgical ablation of atrial fibrillation: recommendations for personnel, policy, procedures and follow-up. *Europace* 9:335–79
72. Danik S, Neuzil P, d'Avila A, Malchano ZJ, Kralovec S, et al. 2008. Evaluation of catheter ablation of periatrial ganglionic plexi in patients with atrial fibrillation. *Am. J. Cardiol.* 102:578–83
73. Haïssaguerre M, Jaïs P, Shah DC, Takahashi A, Hocini M, et al. 1998. Spontaneous initiation of atrial fibrillation by ectopic beats originating in the pulmonary veins. *N. Engl. J. Med.* 339:659–66

74. Haïssaguerre M, Shoda M, Jaïs P, Nogami A, Shah DC, et al. 2002. Mapping and ablation of idiopathic ventricular fibrillation. *Circulation* 106:962–67
75. Stevenson WG, Soejima K. 2007. Interventional cardiac electrophysiology. *Circulation* 115:2750–60
76. Greenspon AJ. 2000. Advances in catheter ablation for the treatment of cardiac arrhythmias. *IEEE Trans. Microw. Theory Tech.* 48:2670–75
77. Di Biase L, Natale A, Barrett C, Tan C, Elayi CS, et al. 2009. Relationship between catheter forces, lesion characteristics, "popping," and char formation: experience with robotic navigation system. *J. Cardiovasc. Electrophysiol.* 20:436–40
78. Satake S, Tanaka K, Saito S, Tanaka S, Sohara H, et al. 2003. Usefulness of a new radiofrequency thermal balloon catheter for pulmonary vein isolation. *J. Cardiovasc. Electrophysiol.* 14:609–15
79. Schmidt B, Antz M, Ernst S, Ouyang F, Falk P, et al. 2007. Pulmonary vein isolation by high-intensity focused ultrasound: first-in-man study with a steerable balloon catheter. *Heart Rhythm* 4:575–84
80. Reddy VY, Neuzil P, d'Avila A, Laragy M, Malchano ZJ, et al. 2008. Balloon catheter ablation to treat paroxysmal atrial fibrillation: What is the level of pulmonary venous isolation? *Heart Rhythm* 5:353–60
81. Mansour M, Forleo GB, Pappalardo A, Heist EK, Avella A, et al. 2008. Initial experience with the mesh catheter for pulmonary vein isolation in patients with paroxysmal atrial fibrillation. *Heart Rhythm* 5:1510–16
82. Reddy VY, Neuzil P, Themistoclakis S, Danik SB, Bonso A, et al. 2009. Visually-guided balloon catheter ablation of atrial fibrillation: experimental feasibility and first-in-human multicenter clinical outcome. *Circulation* 120:12–20
83. Chun KR, Schmidt B, Metzner A, Tilz R, Zerm T, et al. 2009. Cryoballoon pulmonary vein isolation with real time recordings from the pulmonary veins. *J. Cardiovasc. Electrophysiol.* 30:699–709
84. Hardyck CD, Petrinovich LF, Ellsworth DW. 1966. Feedback of muscle activity during silent reading: rapid extinction. *Science* 154:1467–68
85. Searle A, Kirkup L. 2000. A direct comparison of wet, dry and insulating bioelectric recording electrodes. *Physiol. Meas.* 21:271–83
86. Griss P, Tolvanen-Laakso HK, Meriläinen P, Stemme G. 2002. Characterisation of micromachined spike electrodes for biopotential measurements. *IEEE Trans. Biomed. Eng.* 49:597–604
87. Carmo JP, Dias NS, Silva HR, Mendes PM, Couto C, et al. 2007. A 2.4-GHz low-power/low-voltage wireless plug-and-play module for EEG applications. *IEEE Sens. J.* 7:1524–31
88. Gerdle B, Karlsson S, Day S, Djupsjöbacka M. 1999. Acquisition, processing and analysis of the surface electromyogram. In *Modern Techniques in Neuroscience Research*, ed. U Windhorst, H Johansson, pp. 705–55. Berlin: Springer-Verlag
89. Ng WC, Seet HL, Lee KS, Ning N, Tai WX, et al. 2009. Micro-spike EEG electrode and the vacuum-casting technology for mass production. *J. Mater. Process. Technol.* 209:4434–38
90. Ruffini G, Dunne S, Fuentemilla L, Grau C, Farres E, et al. 2008. First human trials of a dry electrophysiology sensor using a carbon nanotube array interface. *Sens. Actuators A* 144:275–79
91. Baek JY, An JH, Choi JM, Park KS, Lee SH. 2008. Flexible polymeric dry electrodes for the long-term monitoring of ECG. *Sens. Actuators A* 143:423–29
92. Chi YM, Jung TP, Cauwenberghs G. 2010. Dry-contact and noncontact biopotential electrodes: methodological review. *IEEE Rev. Biomed. Eng.* 3:106–19
93. Matteucci M, Carabalona R, Casella M, Di Fabrizio E, Gramatica F, et al. 2007. Micropatterned dry electrodes for brain-computer interface. *Microelectron. Eng.* 84:1737–40
94. Stroop JR. 1935. Studies of interference in serial verbal reactions. *J. Exp. Psychol.* 18:643–62

Annual Review of Biomedical Engineering
Volume 14, 2012

Contents

Indexes

Errata

An online log of corrections to *Annual Review of Biomedical Engineering* articles may be found at http://bioeng.annualreviews.org/